13

Demisting Cyclones

Until now we have been concerned with the separation of solid particles from gas streams. However, cyclones may be also utilized quite effectively to separate liquids contained in a carrier gas stream. The principles are the same but liquids pose some unique problems and some advantages relative to solids-collecting cyclones.

We wish to point out at the outset here that, by far, the majority of vapor-liquid separation tasks are performed using either conventional gravity settling or 'knock-out' drums or demisting meshes or pads. Knock-out drums or pots are very robust and are almost always used to separate liquid from carrier gas stream if the incoming stream contains a high volumetric fraction of liquid (greater than several percent). With proper design they can generally be depended upon to separate the majority of droplets greater than about 500 μm but are not suitable for collecting finer droplets. Demisting mats, on the other hand, exhibit relatively low pressure drops (typically less than a few centimeters of water column) and can capture drops as small as a few microns. They are not suitable for high liquid loading conditions such as that which may exists under two-phase slug flow conditions, nor in applications where the demisting mat could be exposed to foam. They are also subject to fouling from any solids or waxy, gummy or coke-forming material in the feed stream.

In between these two separator types are vapor-liquid cyclone separators. Cyclonic type separators have been gaining in importance during the past decade and are now playing a major role in the oil and gas industries, especially in offshore applications where large and expensive gravity separators are being replaced by much more compact, and much more efficient gas-liquid separation equipment. In gas transmission installations cyclones are also well suited to protect gas compressors and turbines from fouling and erosion. In such service they are capable of removing essentially 100% of the solid and liquid particles 6 to 8 microns and larger.

Cyclones, like gravity separators, can be designed to handle large volumetric concentrations of incoming liquid if they are equipped with or set atop

a liquid hold-up drum. As with a gravity separator, such a drum is used to provide liquid level control and, normally, several minutes of liquid surge capacity. Our focus, herein, however, will be on what we shall call 'demisting' cyclones.

Unlike the particles feeding conventional gas-solids cyclones, liquid particles feeding a gas-liquid cyclone are normally greater in size and are not porous. These two factors tend to make for an easier separation. In many systems the gas/liquid mixture feeding the cyclone enters through some upstream piping wherein small droplets coalesce into larger drops, the driving force for the coalescence of colliding droplets being provided by surface tension. We'll present an example of this below. In addition, unlike gas-solids cyclones, once the incoming liquid droplets are centrifuged to the wall of the cyclone, they merge with the liquid wall film to form a much larger mass which is not easily removed or re-entrained back into the gas phase. In gas-solids cyclones, fine dust particles are much more easily re-entrained off the walls. The droplets entering a gas-liquid cyclone are also not likely to plug the cyclone as sometimes occurs with statically charged or tacky solids in a gas-solids cyclone.

In some applications, deposits may form on the roof or outside area of the vortex tube if these surfaces are not sufficiently wetted by the incoming liquid. In these cases, the affected surfaces normally can be kept clean with spray nozzles. Gas-liquid cyclones do not normally pose the same erosion concerns experienced with certain solids handling cyclones. The factors mentioned above – the formation of wall films and their relative immunity to both plugging and erosion – have given their designers more latitude with respect to their construction and design details than that commonly observed with gas-solids cyclones. Thus, demisting cyclones can be found with a wide variety of internal features including relatively thin, close-fitting vanes, narrow slits or shave-offs, anti-creep skirts, isolation disks, coalescing mats, relatively small liquid discharge openings, recirculation slots or slits and attendant piping, and other intricate internals.

13.1 Liquid Creep and 'Layer Loss'

Notwithstanding their many advantages, demisting cyclones also pose a few problems relative to dedusting cyclones. Unlike gas-solids cyclones, some portion of the incoming liquid tends to deposit along the upper walls of the cyclone in the form of a wall film. This wall film is not static or stationary but is driven by the secondary gas flow dragging it up the walls, then radially inwards across the roof, and down the vortex tube. If not redirected, this liquid will simply 'short circuit' the cyclone and exit along with the gas phase. Such behavior, known as 'layer loss', is clearly detrimental to overall separation performance but can be avoided through the use of appropriate 'roof skimmers', vortex-tube 'anti-creep skirts', or inlet 'raceways'. A few such devices are illustrated in Fig. 13.1.1. The raceway functions very much like

the roof-skimming cylinder but attempts to prevent liquid from reaching the upper areas of the cyclone in the first place. The anti-creep skirt often has a serrated or 'saw-toothed' trailing edge to facilitate the dislodging of the liquid film. At high liquid loadings (greater than about 1 kg liquid/kg of gas), both roof skimmer or raceway and an anti-creep skirt should be installed.

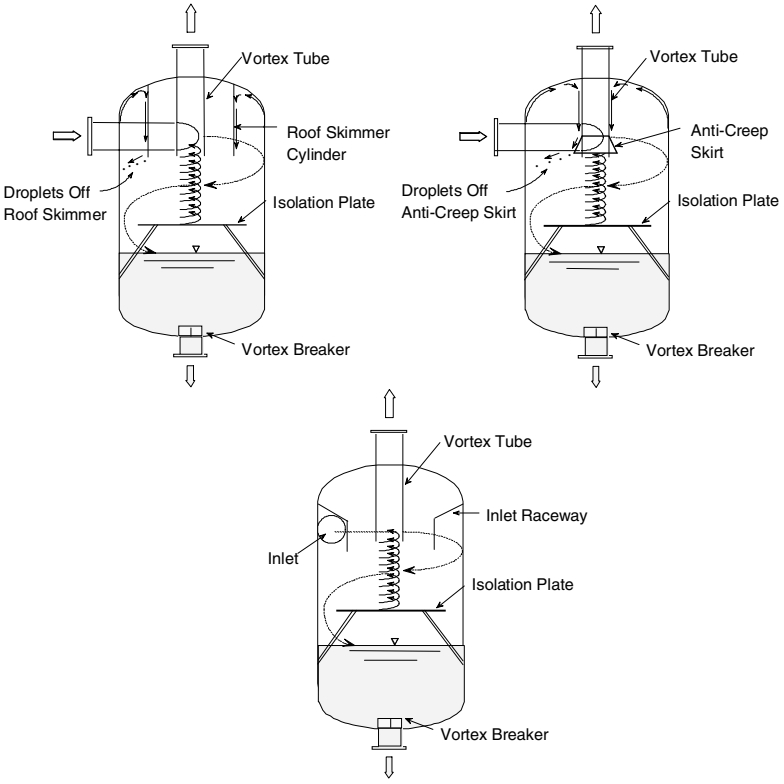

Fig. 13.1.1. Illustration of three vapor-liquid cyclone devices for preventing liquid losses due to secondary flow behavior: roof skimmer, vortex tube anti-creep device and inlet raceway

Unlike their gas-solids cousins, the inlet pipe feeding a vapor-liquid cyclone should not be inserted in very close proximity to the cyclone roof. Nor should it be designed with a 'helical' roof design for gas-liquid cyclones. Both of these configurations tend to encourage the 'layer loss' described above. If possible, the top of the inlet piping should be located at least one inlet pipe diameter below the outside edge of the roof. In principle, at least, it is possible to reduce 'layer losses' by directing the inlet pipe slightly downward (e.g. 10°) although this is rarely observed in practice.

Wherever possible, the inlet piping to a gas-liquid cyclone should consist of a straight section of pipe having a length-to-inside diameter (L/D) ratio not less than 10 following any upstream bends, tees or other flow disturbances. In no case should the L/D ratio drop below 5. Any upstream bend should also cause the two-phase mixture reporting to the cyclone to turn in the same rotational direction as that within the cyclone. For example, if the gas-liquid mixture enters the cyclone in a clockwise manner in plan view, then the nearest upstream bend that lies in a horizontal plane should also make a clockwise turn.

13.2 Demisting Cyclone Design Considerations

Demisting type cyclones are sized following the same general design guidelines reported elsewhere in this book. Unlike gas-solids cyclones, however, the drop size distribution feeding demisting cyclones is generally not very well known. Still, unless the droplets are less than about 10 μm in size, droplets contained in most process streams can be separated with conventional cyclone type separators. This is simply because most cyclones will exhibit a d-50 cut-point diameter between about 3 to 15 μm and the vast majority of droplets contained in process streams (except for 'fogs') are much greater than this. In fact, it is rather difficult to design a cyclone that cannot capture or separate most of the liquid in the majority of applications of commercial interest. The main challenge in such designs lies less with the inherent ability of the cyclone to separate incoming droplets from the gas phase but more with the proper handling of the liquid phase once it is 'centrifuged' to the walls of the separator.

As mentioned above, a vapor-liquid cyclone of the conventional reverse-flow variety must be designed to handle liquid films attempting to make their way out the vortex tube (*i.e.*, 'layer losses'). Additionally, the cyclone must be designed so that the vortex 'tail' (the end of the vortex) is isolated or decoupled from any liquid that is allowed to collect in the lower section of the separator or from the liquid already flowing down the walls. See, for example, Fig. 13.1.1. Furthermore, proper underflow sealing is just as important with vapor-liquid cyclones as it is for gas-solids cyclones.

As an illustration of an underflow seal problem (and related problems), a cyclonic type of droplet separator was once installed on the outlet flange of a very large knock-out drum ahead of a wet-gas compressor (WGC). The separator was equipped with drainpipes that reported down to a pool of liquid and which sealed the drainpipes under normal or design flow conditions. Despite the existence of the knock-out drum and the separator, liquid carry-over from this two-stage separation arrangement led to a major failure of the downstream WGC. Calculations of the separation performance of the cyclonic separator showed that only an insignificant trace of liquid should have escaped the separator for the flow conditions that were in effect at the time of the fail-

ure. In fact, the vapor flow rate was more than double the flow for which the separator was originally designed. This led to a very low computed cut-point diameter for the separator and from this, alone, it appeared as though it was impossible for any significant quantity of liquid to have escaped capture by the separator. Unfortunately, not only was the gas flow through the separator much higher than design conditions originally specified for this service, there was a serious mismatch between the cyclonic separator's gas outlet diameter and the diameter of the gas outlet flange located atop the vessel and to which the separator was directly flanged and in close contact. This smaller diameter outlet flange intensified the swirl and had the same effect that a reduction in vortex tube diameter would have on a conventional cyclone. This produced a pressure loss across the separator that greatly exceeded design expectations. This excessive pressure loss created a suction on the separator's drain pipes sufficient to 'suck' or educt liquid out the bottom of the knock-out drum, through the separator located atop the drum, and into the WGC. Once the true cause of the liquid carryover problem was understood, the limitations with the upstream separation equipment were addressed with the result that not a trace of liquid could be detected at the inlet to the newly rebuilt WGC.

A point we wish to make here is that the ultimate performance of an operating cyclone installation is not just a function of the cyclone design. Rather, the entire 'system' must be examined beyond considerations pertaining solely to droplet aerodynamics and forces acting upon individual droplets. The failure described above was a classic case of what can happen when one limits one's attention to just 'the separator'. There was nothing 'wrong' with the separator, per se, even though it was being operated beyond its design velocities. Likewise, there was nothing 'wrong' with the diameter of the outlet pipe/flange, located atop the vessel, as far as its ability to handle the gas flow through the vessel. But the two, in combination, created the problem described above. The vessel outlet pipe became, in effect, a part of the separator. It's been said that, "Things tend to go wrong at the discipline interfaces." This is true also in the physical 'interfaces' connecting different pieces of equipment; in this case, the separator and the vessel flange.

In two-phase mist-annular flow through ordinary piping, it is observed that the pressure drop through a given section of pipe is greater than that for the gas flow alone. The increase in pressure drop increases very rapidly with increases in liquid loading up to about 0.1 kg liquid per kg of gas. After this, the increase tends to level off rapidly. A film of liquid gives rise to most of the increase in pressure drop. In such cases, the primary reason for the increase in pressure drop is the increased wall roughness created by waves on the surface of the pipe walls. Such is also the case with vapor-liquid cyclones, which may be viewed as operating in a swirling type of 'mist-annular' flow state. In Sect. 13.5 below, we will present an equation for estimating the effect that the liquid phase has on the wall friction factor for gas-liquid cyclones.

13.3 Some Vapor-Liquid Cyclone Design Geometries and Features

Vapor-liquid cyclones come in a bewildering array of design geometries and configurations. The basic design shown in Fig. 13.1.1, and variants thereof, is perhaps the closest thing one can envision as a 'standard' design. Interestingly, most vapor-liquid or demisting cyclones do not feature a conical lower section but tend to be of the cylindrical variety. As shown, it is quite common for vapor-liquid cyclone vessels to function as both a separator and as a liquid holdup vessel. In this capacity, it is quite important – from a separations point of view – that the 'end' of the vortex not be allowed to come in contact with the surface of the liquid pool which exists in the lower part of the cyclone vessel. Hence, an 'isolation' plate (also know as a 'stilling plate' or 'vortex stabilizer plate') is used to provide a surface upon which the end of the vortex can 'lite' and spin like a top. Obviously then the purpose of this plate is not to 'break' or interfere with the vortex but to prevent it from contacting the surface of the liquid phase. Under no conditions should a 'cross' type of device be used to 'break' the main (gas-phase) vortex as these create extreme levels of turbulence and greatly weaken the vortex.

A true 'vortex breaker' is normally inserted just ahead of the vessel's liquid exit nozzle as shown in Fig. 13.1.1. This is a very important feature in the geometry at hand since the angular momentum of the incoming gas-liquid mixture will produce bulk rotation of the liquid pool. If a vortex is allowed to form, some of the incoming gas may exit out the underflow and create pump cavitation or other problems downstream. The vortex will also act as a type of fluidic 'choke' and restrict the flow rate out the bottom liquid exit nozzle.

Vortex breakers normally consist of simple crosses of flat plate metal or a flat circular plate located about 1 outlet pipe diameter above the exit pipe. The plate diameter is normally 2 to 4 times the diameter of the exit pipe. The writers prefer to use both a cross and a wide circular plate in order to prevent a vapor core vortex 'finger' from dipping down and exiting through only one of the 4 open quadrants comprising the vortex cross. Some vortex breakers are "seat of the pants" designs which may, or may not, work. Although there is no one universal standard governing their design, most engineering companies and engineering contractors have "in house" design rules or specifications that cover most design situations one is likely to encounter in practice. This includes vortex breakers for both bottom and side exiting pipes. Pump manufactures are another good source for design assistance.

Aside from installing a vortex breaker on the exiting liquid phase, it is good practice to limit the liquid velocity out the underflow nozzle to a maximum value of about 1 m/s. Downsteam of this nozzle the line size may be reduced to comply with normal pipe sizing criteria or, if solids are present, to prevent their setting out in any horizontal sections of the piping. Consideration should also be given to installing perforated, vertical wall baffles in the liquid phase as these serve to retard bulk rotation of the liquid pool.

Figs. 13.3.1 through 13.3.6 depict several other vapor-liquid cyclone geometries and are somewhat illustrative of the great variety of designs in commercial service. These illustrations are indicative and not exhaustive.

Figure 13.3.1 shows the 'Gasunie' cyclone separator. Note the anti-creep skirts on the vortex finder and the large vortex breaker. The cyclone is of the reverse-flow type and the vanes imparting the swirl to the incoming liquid-laden gas form a fairly shallow angle to the horizontal.

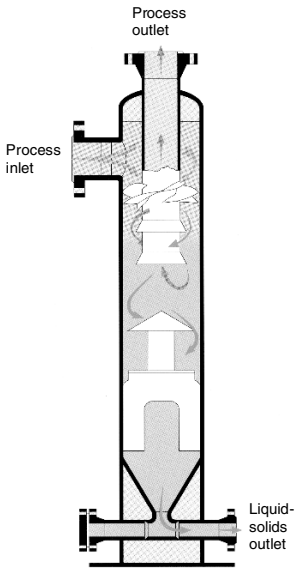

Fig. 13.3.1. Gasunie cyclone separator courtesy of Gasunie Engineering B.V.

Figure 13.3.2 illustrates an 'inline' flange-to-flange reverse-flow cyclone using a stilling plate to isolate the collected liquid from the active vortex. This plate is supported directly off the vessel walls and contains slot-like openings for the liquid to pass through. The vessel's length and/or diameter below the stilling plate may be increased, as necessary, to provide liquid surge or holdup capacity and level control.

Figure 13.3.3 shows a flow-through cyclone that uses a vane type inlet (very common in such flow-through designs) to impart the necessary spin to the incoming gas-liquid mixture. This particular design is very interesting in that it features a demisting mat to first coalesce very fine incoming droplets into larger drops ahead of the cyclone section. We note that the mat does not 'collect' or separate any of the incoming droplets but simply acts to physically enlarge the drop-size distribution. A large ring is attached to the lower end of the vortex tube to help isolate the swirling gas flow from the exiting liquid

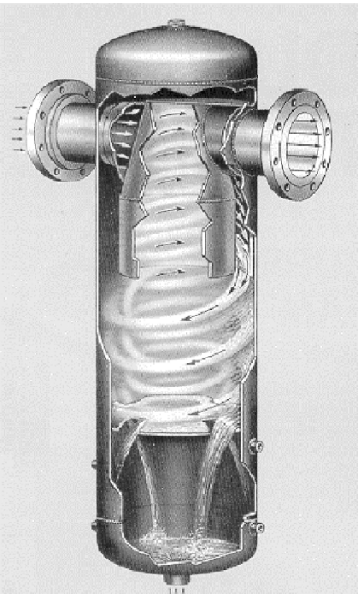

Fig. 13.3.2. Wright-Austin type TS vapor/liquid cyclone separator. Courtesy Hayward Industrial Products, Inc.

phase and to thus facilitate removal of the liquid. A smaller diameter ring is attached near the leading edge of the vortex tube to reduce any 'layer loss' of the type described above. Flow-through cyclones such as this one, or the generic design shown on the right of Fig. 13.3.3 may be designed to operate in either the horizontal or vertical direction. However, it is the writers' opinion that such cyclones perform better in the vertical (down) direction since the arrangement better accommodates gravitational removal of the liquid phase.

As we observed when studying the equilibrium-orbit model of Sect. 5.2, a cyclone's cut size and overall efficiency are dependent upon its diameter. We found that the centrifugal force acting to separate a particle (or droplet, for the case at hand) to the inner walls of the separator is inversely proportional to the radius of the gas outlet pipe, and that the cut size is proportional to the square root of this radius, other factors being equal. Thus, rather than having all the flow report to just one relatively large cyclone, one can achieve an improvement in separation performance by dividing and evenly distributing the flow over a number of small diameter cyclones. A 'multicyclone' (or 'multiclone'), such as that shown in the left-hand side of Fig. 13.3.4, illustrates such an arrangement. It consists of a number of relatively small diameter, cylindrical-bodied cyclones housed in a single pressure-retaining vessel. Two tube sheets are used to isolate the inlet chamber from the upper clean-gas plenum chamber and the lower liquid receiving chamber. The cyclone assembly shown is equipped with liquid level control or sensing taps and a flanged

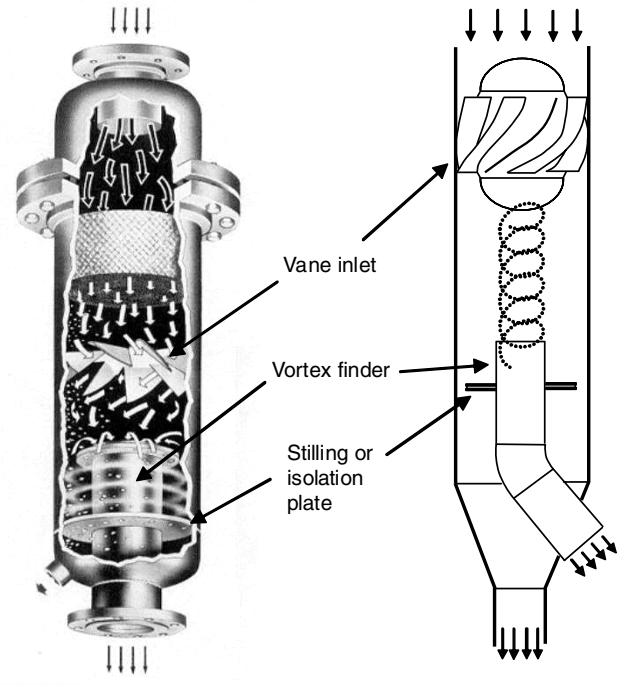

Fig. 13.3.3. Left: Wright-Austin type 31L CLC vapor/liquid cyclone separator. Courtesy Hayward Industrial Products, Inc. Right: A generic flow-through cyclone design

top head for inspection and maintenance access. The three frames to the right of the multiclone vessel illustrate three different designs of the individual cyclone units:

The first features a twin-scroll inlet design, spaced 180 degrees apart, for imparting spin to the incoming gas-liquid mixture. Such twin inlet designs result in a more symmetrical inlet flow pattern relative to the 'slotted inlet' design commonly used in gas-solids separators. They also allow the designer to reduce the overall height of the cyclone body since, for the same total volumetric flow rate, the inlet (a scroll in this case) height is half that of a single inlet design.

The second cyclone body shown in Figure 13.3.4 illustrate a vane-type inlet design that we refer to herein as a swirl tube separator. Vane inlets are the most symmetrical of all inlet designs but are somewhat more complicated to design and fabricate or, in some cases, to cast. Both the twin inlet and vane inlet cyclone designs described thus far are of the conventional reverse-flow variety.

The separator on the far right of Fig. 13.3.4 and in Fig. 13.3.5 is a rather sophisticated cylindrical-bodied flow-through or straight-through type cyclone.

Fig. 13.3.4. A Burgess-Manning multicyclone vapor/liquid separator unit (left-most frame) and three different cyclone body designs: Burgess-Manning type R-T, R-A and A-X, respectively. Courtesy Burgess-Manning, Inc.

Like the aforementioned design, it uses an inlet vane assembly for generating the spin required to separate the incoming liquid (and solids that may be present) to the walls. This separated material is then forced to exit out of a symmetrical array of vertical slots by a purge flow amounting to 15–20% of the incoming gas flow. This purge stream is recycled back into the separator though a hollow pipe, which also supports the inlet vane, see Fig. 13.3.5. The relatively low static pressure that exists in the vortex core is what drives this recirculating gas flow. The liquid (and solids, if present) that exits the slots with the purge flow report to the liquid pool at the bottom of the vessel. Figure 13.3.5 also illustrates the use of a 'half-pipe' vessel inlet design often used to remove any large drops or incoming liquid slugs ahead of the multicyclone assembly.

Because they can more effectively separate smaller droplets relative to a conventional, large, single-stage cyclone, multiclones are reported to have 'turn-down ratios' (maximum-to-minimum volumetric feed rate that still meets performance targets) as high as 4:1.

Strong similarities exist between gas-solid and gas-liquid cyclones and, thus, the reader may wish to review the related discussion presented in Sect. 16.2 pertaining to gas-solid multiclone separators.

Scrubbing type cyclones use features of both a dry cyclone and a spray chamber to remove pollutants[1] or particulates from a gas stream. This type

[1] In this text, we distinguish "pollutants" from "particulates", recognizing that not all particles (liquid or solids) are "pollutants". In most industrially important operations particles are captured for recycling back to the process from which

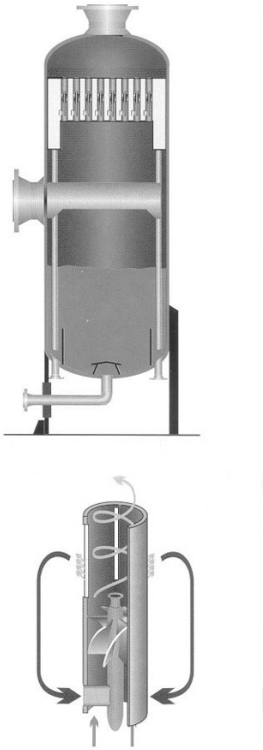

Fig. 13.3.5. A Burgess-Manning separator vessel (top frame) equipped with type A-X recycling type multicyclones (bottom frame). Courtesy Burgess-Manning, Inc.

of technology is a part of the group of air pollution or particulate collection devices collectively referred to as wet scrubbers.

Figure 13.3.6 is a photograph of a skid-mounted venturi-scrubber/cyclone separator system. Spray water injected (see far left-hand side in the photograph) is captured by the rather short cylindrical-bodied cyclone separator located immediately downstream of the scrubber. We note that the cyclone has a scroll-type rectangular inlet and that the downstream blower makes this a pull-through type system. Scrubber water collected by the cyclone reports to a receiving tank located below the cyclone. From here, it is pumped back up through the scrubber's spray nozzles.

The two cyclonic scrubbers shown in Fig. 13.3.7 are capable of removing particulates as small as 2 to 3 microns as well as any gaseous components that are soluble in water. They typically operate at liquid-to-gas (L/G) ratios of 0.3 to 1.3 l/m^3 (2 to 10 gal/1000 ft^3) and at pressure drops of 4 to 25 cm

they came or they are the product or byproduct themselves. In some situations both definitions fit.

Fig. 13.3.6. A skid-mounted venturi scrubber/cyclone ensemble by Fisher-Klosterman, Inc.

of water (1.5 to 10 in. of water). They are often utilized in mining, drying, foundries, and food processing industries.

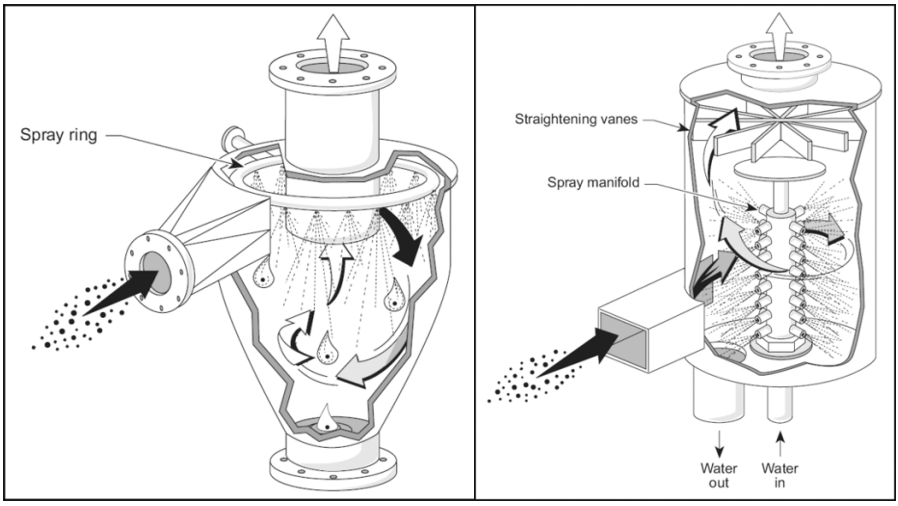

Fig. 13.3.7. Left: an irrigated cyclone scrubber. Right: a cyclonic spray scrubber. Source: US Environmental Protection Agency

Unlike simple spray towers that operate at gas velocities on the order of 0.6 to 1.5 m/s (2 to 5 ft/s), cyclonic scrubbers are designed to operate at gas velocities of 60 to 180 m/s (200 to 600 ft/s). This makes cyclonic scrubbers much more efficient than spray towers in removing particulates due to the much greater particle-to-liquid relative velocity and turbulence. However, cyclonic type scrubbers are still not as efficient as venturi scrubbers.

Although cyclonic scrubbers are relatively compact and quite robust, due to their high gas velocities, they must sometimes be equipped with special abrasion-resistant liners to control the rate of erosion, especially in their inlet target zones. Aside from erosion, corrosion can also be a concern since most structural alloys corrode from exposure to moisture in the air or gas stream. Corrosion is of special concern if the gas contains agressive constituents such as acids, caustics, dehydrating agents, halogens and halogen salts, organic halides, carbolic acid, etc.

Spray nozzle plugging is another concern. Nozzles have a tendency to plug either due to particles in the water recycle stream or in the gas stream. Nozzles can also erode internally due to particles in the recycle water. They can also corrode. Strainers are usually required to protect the nozzles from such internal erosion. In any case, the design of the spray header should be such that the nozzles are accessible for routine cleaning or replacement.

The design of cyclonic scrubbers is usually based on pilot tests, experience with units in similar service and empirical correlations rather than any fundamental model of absorption or particle collection performance. A skid mounted test unit, similar to that shown in Fig.13.3.6, can give plant personnel a very good indication of the expected performance of a commercial scale unit.

13.4 Estimating Inlet Drop Size for Two-Phase Mist-Annular Flow

Unlike a solids collecting cyclone, the performance of a demisting cyclone is much more dependent upon the flow conditions that exist in the upstream piping. This, of course, is because the 'particle' or drop size distribution feeding the cyclone is strongly dependent upon such factors as shear rate and surface tension. The shear rate is, itself, a function of the upstream pipe diameter, the superficial gas velocity and the physical properties (namely densities and viscosities) of the gas and liquid phases.

Under mist or mist-annular flow conditions, such as that illustrated in Fig. 13.4.1, one can use the 'Harwell' technique to get a rough estimate of the average drop size (UKAEA, 1980).

The Harwell procedure applies to steady-state flow conditions and to the flow pattern existing downstream of any flow disturbances (such as orifice plates, valves, expanders, bends, tees, etc.). It is only one of several correlations available for computing drop sizes. Nonetheless, it was developed on

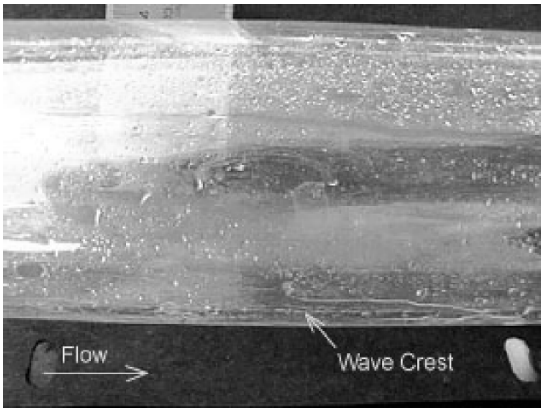

Fig. 13.4.1. Mist flow in a horizontal 2 inch ID pipe. Note small wave crest at bottom center of pipe

basis of many steam-water, air-water and other fluid data and, because of this, it is considered by the writers to be one of the more accurate and robust correlations available.

Harwell's method for predicting average drop size contains two additive terms. One is dependent upon the volumetric concentration of droplets in the gas phase and the other is independent of the droplet concentration. However, the concentration dependent term is rather difficult to estimate a priori and we will not include it here. When this term is neglected, the average drop size computed will tend to be somewhat smaller than that which we would expect to experience in practice. This approach is normally quite acceptable from a separator sizing or evaluation point of view since any droplets larger than what we may compute are those that are most easily separated.

The Harwell equation predicts that the 'Sauter mean' (the mean of the surface distribution rather than the volume distribution, see Chap. 2) droplet diameter is:

$$\langle x \rangle_{Sa} = 1.91 D_t \frac{Re^{0.1}}{We^{0.6}} \left(\frac{\rho}{\rho_l} \right)^{0.6} \tag{13.4.1}$$

where Re and We are the Reynolds and Weber number, respectively. They are defined as,

$$Re = \frac{\rho v_t D_t}{\mu}, \quad We = \frac{\rho v_t^2 D_t}{\sigma}$$

and where $\langle x \rangle_{Sa}$ is the Sauter mean droplet diameter. D_t is the internal diameter of the pipe, ρ and ρ_l are the gas and liquid densities, μ is the gas viscosity, v_t is the mean gas velocity within the pipe and σ is the interfacial surface tension ('IFT')

The Weber number can be understood as the ratio of inertial forces, which tend to break a droplet apart, and surface tension forces, which tend to hold it together.

In certain mass-transfer operations, such as spray columns, the Sauter mean diameter is a useful quantity to know. However, in studies of droplet erosion or droplet separation, the volume or mass median diameter is more physically meaningful. This volume-average (median) drop diameter is related to the Sauter-mean diameter through the following approximation (AIChE, 1978).

$$\langle x \rangle_{med} = 1.42 x_{Sa}. \tag{13.4.2}$$

An example calculation for estimating the Sauter mean droplet size in pipelines is included in Appendix 13.A.

13.4.1 Estimating Drop Size Distribution

The preceding section provides us with a technique for estimating the volume-averaged drop size of a collection of droplets flowing within a pipe under mist-annular flow conditions. And while this is often all that one may wish to know about the droplet distribution, it is sometimes of interest to know, or at least estimate, the entire drop size distribution. Such would be the case if one wished to perform a cyclone simulation study which required, as input, an estimate of the inlet drop size distribution which may exist within the upstream pipe feeding the cyclone.

Fortunately, it turns out (AIChE, 1978) that the width of the drop size distribution is strongly dependent upon the volume or mass average droplet size, x_{med}, as previously computed. Furthermore, if the drop size distribution [*i.e.*, $F(x)$] is normalized by dividing each x by x_{med}, then, as a rough approximation, all droplet distributions are identical and can be represented as shown in Table 13.4.1 and 13.4.2:

Table 13.4.1. Points on the standard size distribution for droplets

x/x_{med}	0	0.3	0.62	1	1.5	2.9
$F(x/x_{med})$	0	0.05	0.25	0.5	0.75	1.0

For this distribution the mean size $\langle x \rangle$ is almost equal to the median size x_{med}.

We may note that:

- only about 5% of the droplets will be of size $x/x_{med} = 0.30$ or less
- 100% will be less than $x/x_{med} = 2.9$

In Appendix 13.A, an example calculation showing how to use this standard droplet distribution is given.

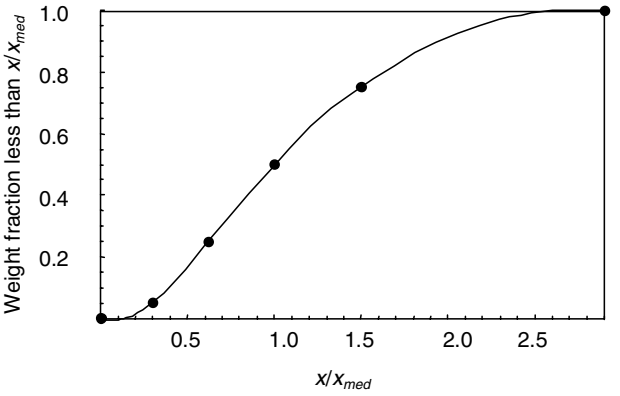

Fig. 13.4.2. Standard size distribution for droplets in pipelines

13.5 Modeling the Performance of Vapor-Liquid Cyclones

The method we wish to present here for modeling the performance of vapor-liquid ('demisting') cyclones follows closely the method presented by Muschelknautz and Dahl (1994) and that presented for gas-solids cyclones previously reported in Chap. 6. All the same, to avoid repetition of the formulism, here we shall focus on pointing out differences in the two methods. The reader is encouraged to refer back to Chap. 6 while reading the discussion below.

The calculation method reported below is rather rudimentary in comparison to that which we have reported earlier for gas-solids cyclones. There is still substantial room for further refinement in the modeling of vapor-liquid cyclones.

Unlike their gas-solids counterparts, one almost never knows from measurement the droplet size distribution feeding vapor liquid cyclones and, quite often, one is often not certain of the quantity of liquid feeding the cyclone. Still, the method presented below should provide some help as it provides a rough method for estimating the cyclone's cut size and, if the liquid loading and its approximate distribution is known, the overall collection efficiency.

The equations assume that the cyclone is constructed with a roof skimmer or raceway and a vortex tube anti-creep skirt to minimize the detrimental effects of liquid creep, as well as a vortex stabilizing plate to prevent collected liquid from becoming re-entrained.

13.5.1 Computation of Cut Size

As was the case for gas-solids cyclones, we begin by computing the entrance 'constriction' coefficient, α, from Eq. (6.1.1). If, as is often the case for vapor-liquid cyclones, the entrance duct is a circular pipe, the 'width' variable, b,

appearing in the formula $\xi = b/(\frac{1}{2}D) = b/R$, is to be interpreted as the inside diameter of the cyclone's inlet pipe, d_e. In addition, the inlet loading variable, c_o, is now defined as the ratio of the mass of incoming *liquid* to mass of incoming gas in the feed stream.

We compute the tangential velocity of the gas at the 'inner core' radius, R_{CS}, by following the calculation procedure leading up to Eq. (6.2.1) and by using the same equation reported therein for the frictional area term,A_R. However, for the computation of the total friction factor, f, we do not use Eq. (6.1.11) but the simpler, approximate expression geared to liquids:

$$f = f_{air}\left(1 + 0.4c_o^{0.1}\right) \tag{13.5.1}$$

where, as before, f_{air} is the gas-only friction factor computed from Fig. 6.1.3. The term in parenthesis above is a liquid-loading correction factor to the gas-only friction factor. It varies in magnitude from 1, at negligible loadings, to 1.4 at a inlet loading of 1.0. Its dependency upon loading is very weak beyond a loading of about 0.1. That is, a thicker film of liquid on the wall does not offer much more resistance to flow than a thinner film.

The all-important cut size or cut-point diameter of the inner vortex may now be computed directly from Eq. (6.2.3) or, if necessary, Eq. (6.2.6) where the particle density, ρ_p, now refers to the density of the liquid phase.

13.5.2 Computation of Efficiency at Low Inlet Loadings

In this section we will compute the grade-efficiency curve and overall separation efficiency at low inlet loadings ($c_o < c_{oL}$)—the classification-only case.

The grade-efficiency curve one uses to quantify separation efficiency as a function of particle (drop) size should be based on experimental data or plant measurements taken on a cyclone of similar design and operation. However, lacking such information, we suggest, as before, using Eq. (6.3.2) with a 'slope', m, of about 3.

Overall collection efficiency is again computed from Eq. (6.3.3) by summing up the efficiencies of the individual size fractions, weighted by their mass fraction in the incoming feed.

13.6 Criteria for Determining if 'Mass loading' ('Saltation') Occurs

In analogy to our gas-solids cyclones, the amount of liquid that the gas phase can hold in turbulent suspension upon its entrance into a cyclone depends on the mass average drop size of the feed, $\langle x \rangle$, the cut-point of the 'inlet wall region', x_{50in}, and, to a lesser extent, the inlet loading itself, c_o. For gas-liquid cyclones, Muschelknautz and Dahl (1994) report for the limit-loading concentration:

$$c_{oL} = 0.0078 \left(\frac{x_{50in}}{\langle x \rangle} \right) (10 c_{ok})^k \qquad \text{for } 0.01 < c_{ok} > 0.5 \qquad (13.6.1)$$

where

$$k = 0.07 - 0.16 \ln c_{ok} \qquad (13.6.2)$$

and where c_{ok} is the mass of liquid *suspended* in the incoming gas stream per unit mass of gas. However, introducing the quantity x_{50in} complicates the analysis considerably. Furthermore, our calculations show that x_{50in} is typically only about 25% greater than the cut size of the inner vortex, x_{50}, calculated by Eq. (6.2.3). For these reasons, we will substitute $x_{50}$for x_{50in} and rewrite Eq. (13.6.1) as,

$$c_{oL} = 0.0078 \left(\frac{x_{50}}{\langle x \rangle} \right) (10 c_{ok})^k \qquad \text{for } 0.01 < c_{ok} > 0.5. \qquad (13.6.3)$$

As mentioned above, c_{ok} is the mass of liquid *suspended* in the incoming gas stream per unit mass of gas. As such, it will always be less than the total liquid loading since some portion of the incoming liquid will always enter the cyclone as 'wall flow'. Yet, in most practical applications, we do not know c_{ok} since it is difficult or impractical to either measure in an operating plant or to predict, in general, from fluid flow considerations. However, if we use the total incoming liquid loading, c_o, in place of the suspension loading,c_{ok}, in Eq. (13.6.3), the result will be 'conservative' as far as overall separation efficiency is concerned. This is because the actual limit-loading will, in reality, be less than that computed using the total entrance liquid loading, c_o, and any liquid entering the cyclone in excess of c_{oL} will be captured immediately upon entrance. Thus, we shall use the total liquid loading, c_o, in Eq. (13.6.3) knowing that our estimate of the amount of liquid that may be captured because it exceeds the limit-loading will be a conservative one. In the event that the incoming liquid loading exceeds 0.5, we recommend using 0.5 for c_{ok} in Eq. (13.6.3).

If $c_o < c_{oL}$, then there is no 'mass loading' effect and the comparatively simple method for computing the cyclone's separation performance, as described in Sects. 13.5.1 and 13.5.2, applies. Conditions that may lead to this scenario include a low liquid loading, c_o, a very fine feed drop size distribution, and a large inner vortex cut-point diameter, x_{50}.

If $c_o > c_{oL}$, then 'mass loading' will occur and the cyclone will, in effect, become a two-stage separator: separating a portion of the incoming liquid immediately upon its entrance into the cyclone and a portion of the remaining liquid via classification in the spinning inner core.

13.6.1 Overall Separation Efficiency when $c_o > c_{oL}$

As we reported for gas-solids cyclones, the overall or total efficiency for gas-liquid cyclones under mass loading or saltation conditions also includes a

'saltation' and a 'classification' contribution. A portion of the incoming liquid that is not collected by the former is collected by the latter, so that the total efficiency becomes:

$$\eta = \left(1 - \frac{c_{oL}}{c_o}\right) + \left(\frac{c_{oL}}{c_o}\right) \sum_{i=1}^{N} \eta_i \times \Delta MF_i \tag{13.6.4}$$

where, again, ΔMF_i is the i^{th} mass fraction and η_i is the capture efficiency for the i^{th} size fraction computed via Eq. (6.3.2) with x_{50} obtained from Eq. (6.2.3).

13.7 Re-entrainment From Demisting Cyclones

Although re-entrainment, as mentioned in the beginning of this chapter, is much less of a problem in demisting than in dedusting cyclones, demisting cyclones are in some practical applications operated at such severe conditions that re-entrainment does, nevertheless, become the limiting factor for separation. For example, with the push to process natural gas under high gas and liquid loads and at high pressure, the physical properties of the gas and liquid are becoming more challenging in terms of separation efficiency. Also for gas processing off-shore and sub-sea the accuracy and robustness of models predicting the separation efficiency is more crucial, since the consequences of equipment failure are more severe in such applications.

13.7.1 Re-entrainment Mechanisms and Governing Parameters

Only little work focusing on high liquid loading in, and re-entrainment from, demisting cyclones has been published, although some is beginning to emerge in the research literature. Ng et al. (2006) studied flooding phenomena in, and entrainment from, once-through swirl tubes with upflow. They installed and tested radical design improvements to the swirl vanes, using vanes with peripheral rather than axial inflow, to significantly delay the onset of flooding and entrainment.

Below we give a short account of some work that has been done in one of the author's (Hoffmann) own research group (Austrheim, 2005) in the framework of the HiPGaS (High Pressure Gas Separation) project, which sheds some light on the nature of the phenomenon of re-entrainment, and points the way to the formulation of predictive models.

Re-entrainment from cyclones may take place due to droplet entrainment from the film of separated liquid on the cyclone wall close to the exit from the cyclone, or from some edge at the outlet. We focus on the former, and assume that if re-entrainment takes place from an edge rather than a wall, the parameters governing the process will be the same or similar.

Different mechanisms of entrainment from a liquid film on a wall dominate in different film flow regimes. In a classic paper, Ishii and Grolmes (1975) summarize four basic mechanisms for entrainment from a liquid film into a gas flowing co-currently above it. The two that are likely to be relevant in demisting cyclones are illustrated in Fig. 13.7.1.

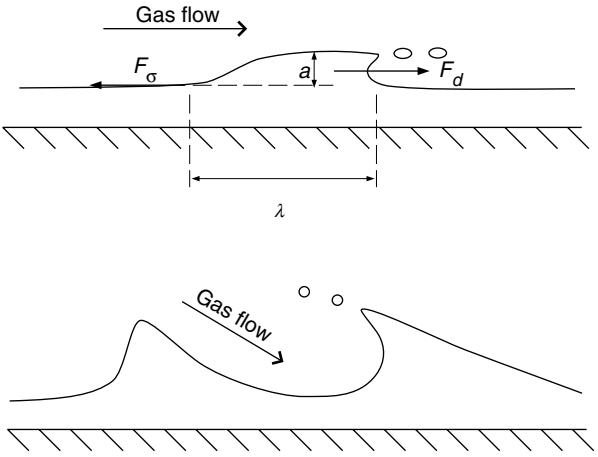

Fig. 13.7.1. Two mechanisms Ishii and Grolmes (1975) report for entrainment from a liquid film into a gas flowing over it. Top: entrainment by droplets being sheared from the surface of a roll wave, which is dominant at higher film Reynolds numbers. Bottom: entrainment by the gas undercutting a wave crest, which dominates at low film Reynolds numbers

The flow regime in the film depends on the film Reynolds number:

$$Re_l \equiv \frac{\rho_l u_l \delta}{\mu_l} = \frac{\rho_l \Gamma}{\mu_l} \tag{13.7.1}$$

where δ is the thickness of the film, u_l its mean velocity and ρ_l and μ_l the density and viscocity of the liquid, respectively. Γ is the liquid flow in the film per unit wetted perimeter, P_w, and is sometimes called the "liquid loading", but in this book we reserve that term for the volumetric liquid concentration in the droplet-laden gas flow.

The film flow regime relevant in the work of Austrheim (2005) is the regime corresponding to intermediate or high Re_l, where the so-called "roll-wave" entrainment dominates: waves on the liquid film are sheared as shown in the top plate of Fig. 13.7.1. The figure also illustrates the strategy of Ishii and Grolmes for modeling this process. They considered a force balance between the drag force F_d , from the gas acting on a wave crest on the film, and the retaining force of the surface tension F_σ as indicated in Fig. 13.7.1. They

considered that roll wave entrainment would take place when the drag force exceeds the retaining force:

$$F_d \geq F_\sigma. \tag{13.7.2}$$

We have to refer to their paper for the details of the derivation, but their criterion for the onset of entrainment is:

$$\begin{aligned} \frac{\mu_l u_g}{\sigma}\sqrt{\frac{\rho_g}{\rho_l}} &\geq 11.78 N_\mu^{0.8} Re_l^{-1/3} \qquad \text{for} \quad N_\mu \leq \frac{1}{15} \\ \frac{\mu_l u_g}{\sigma}\sqrt{\frac{\rho_g}{\rho_l}} &\geq 1.35 Re_l^{-1/3} \qquad \text{for} \quad N_\mu \geq \frac{1}{15} \end{aligned}. \tag{13.7.3}$$

We mention that at high values of Re_l, the criterion becomes independent of Re_l, and therefore simpler. In Eq. (13.7.3), N_μ is a "viscosity number", which measures the ratio of the viscous force due to the internal flow in the wave to the force due to surface tension:

$$N_\mu \equiv \frac{\mu_l}{\sqrt{\rho_l \sigma \sqrt{\frac{\sigma}{g\Delta\rho}}}}, \tag{13.7.4}$$

where $\Delta\rho$ is the difference between the liquid and gas densities.

In applying this to cyclone demisters, Austrheim (2005) assumed that the cyclone efficiency, *when limited by re-entrainment*, is a function of the *ratio* of F_d and F_σ, such that the efficiency can be written:

$$\eta_{entr}(a) = \mathrm{f}\left(\frac{\frac{\mu_l u_g}{\sigma}\sqrt{\frac{\rho_g}{\rho_l}}}{N_\mu^a Re_l^{-1/3}}\right), \tag{13.7.5}$$

calling the group on the right-hand-side the *re-entrainment number*. Ishii and Grolmes (1975) and Austrheim (2005) adjusted the value of the exponent a to optimize the performance of their models, Austrheim finding the optimal value to be 0.4.

The Reynolds number of the film, which is swirling around the wall of a cyclone, was calculated as:

$$Re_l = \frac{\rho_l u_l \delta}{\mu_l} = \frac{\dot{Q}\eta\rho_l}{P_w \mu_l} \tag{13.7.6}$$

where P_w is taken as $\pi D/\cos\alpha$. $\dot{Q}$ is the total liquid flow to the cyclone, η is the fraction separated to the wall and α is the angle to the horizontal of the liquid flow. The latter is taken as equal to the angle to the horizontal at which the *gas* flows, which again, in the vaned swirl tube used by Austrheim, is taken as equal to the exit angle, β, of the vanes.

Since the liquid film in cyclones is swirling around the wall rather than running along the wall in a gravity field, g in Eq. (13.7.4) needs to be replaced

by the centripetal acceleration of the film, which is the square of the tangential film velocity divided by the radius of the cyclone wall, $u_{\theta,l}^2/R$.

This makes it necessary to determine $u_{\theta,l} = u_l \cos\alpha$, where u_l is the absolute velocity in the liquid film. By a procedure similar to that used by Ishii and Grolmes (1975), Austrheim (2005) derives the following expression for $u_{l,\theta}$:

$$u_{l,\theta} = \sqrt{\frac{f_{g,i}\rho_g u_{g,\theta}}{f_{l,w}\rho_l}}, \tag{13.7.7}$$

where $f_{g,i}$ and $f_{l,w}$ are the friction factors between the gas and the liquid film surface and the liquid film and the wall, respectively, found from:

$$f_{g,i} = 0.005\left(1 + 300\frac{\delta}{R}\right)$$
$$\sqrt{f_{l,w}} = K \cdot Re_l^m \text{ where: } \begin{cases} K = 3.73; m = -0.47 & \text{for } 2 < Re_l < 100 \\ K = 1.96; m = -1/3 & \text{for } 100 < Re_l < 1000 \end{cases} \tag{13.7.8}$$

Finally, to calculate $f_{g,i}$, we need δ, the thickness of the liquid film, which is calculated as:

$$\delta = \frac{\dot{Q}}{P_w u_l} = \frac{\dot{Q}\cos\alpha}{P_w u_{l,\theta}} = \frac{\dot{Q}\cos^2\alpha}{\pi D u_{l,\theta}} \tag{13.7.9}$$

$u_{\theta,l}^2/R$ should thus replace g in Eq. (13.7.4) when calculating N_μ for use in Eq. (13.7.5).

As an aside, we can mention at this point that, as an alternative to the dimensionless parameters of Ishii and Grolmes (1975), van Rossum (1959) used the *Weber number* for the liquid film, with the film thickness as length scale, and a *"correlation parameter"*, S:

$$We \equiv \frac{\rho_g v_g^2 \delta}{\sigma} \qquad S \equiv \frac{u_g \mu_l}{\sigma} \tag{13.7.10}$$

to correlate data for the inception of entrainment from a liquid film. For velocities higher than 25 m/s he found that the critical Weber number for inception of entrainment was practically independent of S for $S > 5$, while it became dependent on S for lower S-values.

13.7.2 Data for Re-entrainment

Data for the efficiency of a cyclone bank were obtained in an experimental model of a gas scrubber, incorporating also an inlet vane and a mist mat or demisting mesh under the cyclone "bank", which consisted of two cyclones operating in parallel. A simple diagram of the scrubber is shown in Figure 13.7.2.

The model (called the"high-pressure rig") could be operated at pressures up to 100 bar. The fluids used in the rig were:

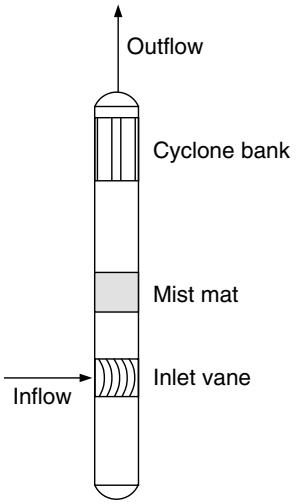

Fig. 13.7.2. Diagram of the scrubber tested by Austrheim (2005)

- air/Exxsol D60, Exxsol D60 is a commercial hydrocarbon liquid
- a synthetic "live" natural gas system, the gas being synthesized from methane, ethane and N-pentane.

Figure 13.7.3 shows the raw efficiency data plotted against superficial air velocity in the cyclones. The fact that the efficiency reduces with increasing gas velocity confirms that re-entrainment, and not separation efficiency of the incoming droplets, is the factor limiting the cyclone separation efficiency.

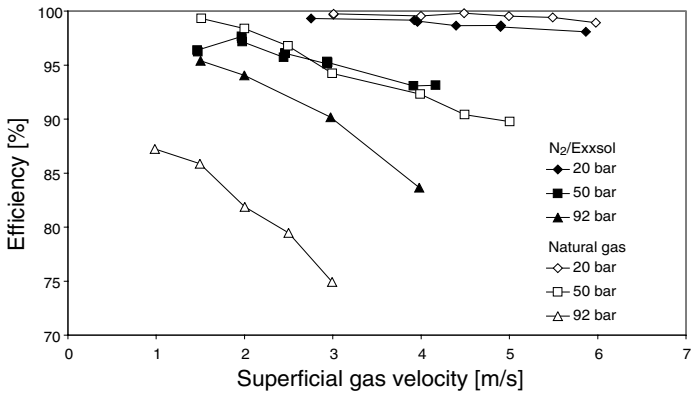

Fig. 13.7.3. Cyclone efficiency in the high-pressure rig with a constant liquid flowrate to the cyclones of 45 l/hr per cyclone

Figure 13.7.4 shows the same data as in Fig. 13.7.3 plus some additional ones at other liquid loadings (the liquid loadings were in the range 9–73 l/hr per cyclone) plotted against the re-entrainment number. In fact, to optimize this plot not only the exponent a was optimized but also the power of (ρ_g/ρ_l), which was made 0.8 rather than the 0.5 of the original model of Ishii and Grolmes (1975).

Plotting the data against this modified re-entrainment number clearly brings all the results onto one line, giving hope that the re-entrainment number can form the basis for a model of re-entrainment in cyclones.

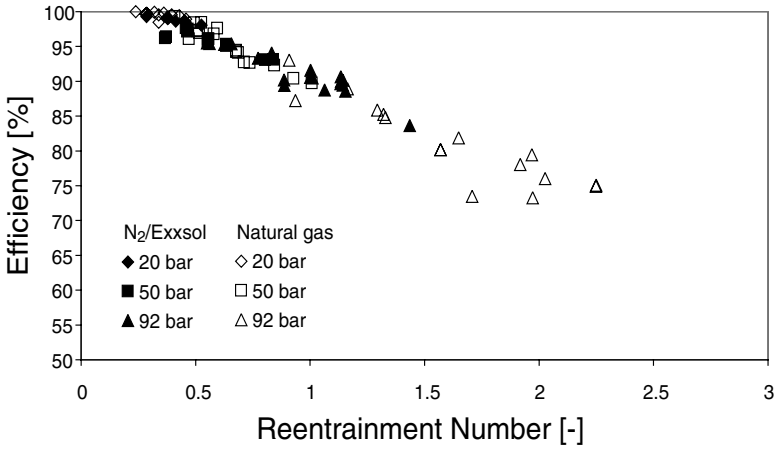

Fig. 13.7.4. The cyclone efficiency plotted agianst the modified re-entrainment number $([\mu_l u_g/\sigma][\rho_g/\rho_l]^{0.8})/(N_\mu^{0.4} Re_l^{-1/3})$

We stress, however, that this is still in the research stage. Figure 13.7.5 incorporate also results obtained from another rig ("low-pressure rig") operating from 1–7 bar on two fluid systems: air/water and air/Exxsol. These new results were also very scattered when plotted against the superficial gas velocity, but are also clearly brought onto one line by plotting against the re-entrainment number. However, the two lines representing the two rigs do not coincide, although perhaps the onset of re-entrainment does take place at the same value of the re-entrainment number in both rigs.

It turns out that also the film Weber number, Eq. (13.7.10), is successful in bringing some of the results onto one line.

It thus seems that these parameters are promising for the formulation of a model for re-entrainment in demisting cyclones. We are of the opinion that the formulation of such a comprehensive model should be an important research priority for the near future, particularly in light of the intensifying interest in off-shore, subsea natural gas processing.

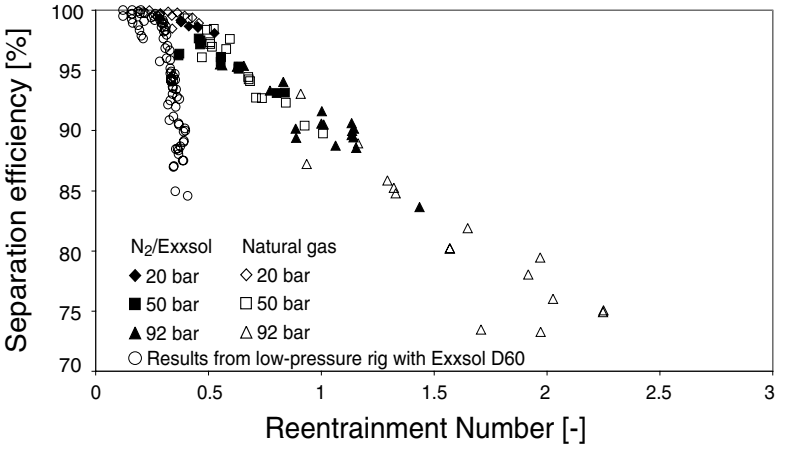

Fig. 13.7.5. A comparison between the cyclone efficiency in the high-pressure and the low-pressure rigs in terms of the modified re-entrainment number $([\mu_l u_g/\sigma][\rho_g/\rho_l]^{0.8})/(N_\mu^{0.4} Re_l^{-1/3})$. The data from the low-pressure rig include cyclone superficial gas velocities in the range 6–30 m/s and liquid loads in the range 0.002–0.09 vol%

13.A Example Calculations of Droplet Sizes in Pipe Flow

13.A.1 Finding the Mean Droplet Size

A gas having a density of 13 kg/m^3 and a dynamic viscosity of 0.006 cp flows through a pipe of 30 cm internal diameter at 6.7 m/s. Entrained in this gas is a liquid hydrocarbon having a density of 930 kg/m^3. A two-phase flow map indicates mist-annular flow. The interfacial tension (or 'IFT') = 20 dynes/cm.

Compute the Sauter-mean and volume-mean droplet diameters.

Solution

To convert to a consistent set of units, we elect to express the IFT and the gas viscosity in SI units:

$$\sigma = 20 \text{ dynes/cm} \times 0.001(\text{N/m})/(\text{dyne/cm}) = 0.02 \text{ N/m}$$

$$\mu = 0.006 \text{ cp} \times 0.001(\text{Pa s})/(\text{cp}) = 6 \times 10^{-6} \text{ Pa s}$$

Thus,

$$Re = \frac{\rho v_t D_t}{\mu} = \frac{13 \times 6.7 \times 0.3}{6 \times 10^{-6}} = 4.4 \times 10^6$$

and

$$We = \frac{\rho v_t^2 D_t}{\sigma} = \frac{13 \times 6.7^2 \times 0.3}{0.02} = 8.87 \times 10^3.$$

Substituting the above two dimensionless ratios, along with the pipe diameter and density values into Eq. 13.4.1, we obtain,

$$\langle x\rangle_{Sa} = 1.91 d_t \frac{Re^{0.1}}{We^{0.6}} \left(\frac{\rho_g}{\rho_l}\right)^{0.6} = 1.91 \times 0.3 \times \frac{\left(4.4 \times 10^6\right)^{0.1}}{\left(8.87 \times 10^3\right)^{0.6}} \left(\frac{13}{930}\right)^{0.6}$$
$$= 8.7 \times 10^{-4} \text{ m} = 870 \ \mu\text{m}$$

and, from Eq. (13.4.2), the volume or mass average droplet size is estimated to be,

$$x_{med} = 1.42 \times 870 \cong 1300 \ \mu\text{m}.$$

Thus, by weight or by volume, approximately 50% of the droplets flowing in the pipe will be smaller than, and 50% larger than, 1300 μm or 1.3 mm.

13.A.2 Finding the Droplet Size Distribution

In the above example we found that $x_{med} = 1300$ μm. Knowing x_{med}, we can therefore compute x for various x/x_{med} ratios for which the various weight fractions smaller than x are known.

$$x = \frac{x}{x_{med}} x_{med}.$$

Values of the droplet diameter computed by the above equation are reported in the second row of Table 13.A.1 and shown in Fig. 13.A.1.

For this computed drop size distribution only about 5% of the drops will be less than 390 μm in diameter and virtually all will be less than 4 mm (4000 μm).

Table 13.A.1. Points on the size distribution of the droplets in the pipe

x/x_{med}	0	0.3	0.62	1	1.5	2.9
x, μm	0	390	806	1300	1950	3770
F(x/x_{med})	0	0.05	0.25	0.5	0.75	1.0

13.B Flow Distribution in Parallel Demisting Cyclones

Figure 13.B.1 depicts a parallel ('multicyclone') arrangement of six demisting cyclones, with each cyclone discharging its overhead vapors into a common attic chamber and its underflow liquid into a common pool of liquid. The two 'front' cyclones take their feed from the near-wall regions of the inlet duct. The two 'back' cyclones take their feed from the centermost section of the inlet ducting. The 'middle' cyclones take their feed from that section of the inlet

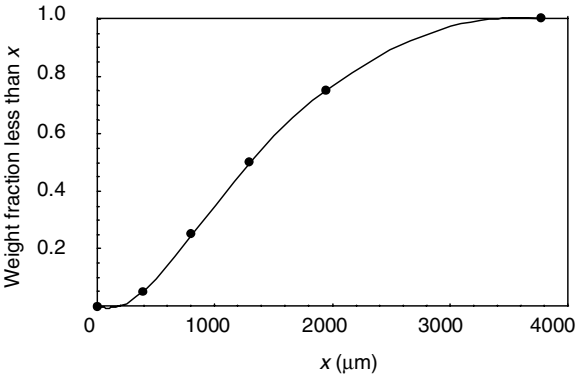

Fig. 13.A.1. Estimated drop size distribution for the example problem on basis of the AIChE design technique

ducting that lies between the wall and the middle of the entrance duct. Since wall friction retards the flow near the two sidewalls of the inlet ducting, the two front cyclones experience a slightly lower impact pressure than either the middle or back cyclones. This forces more vapor to flow into the back cyclones than to the two front cyclones. (Note, in this analysis, and for simplicity sake, we will focus attention on the two 'front' and 'back' cyclones.) This somewhat greater vapor flow to the two back cyclones produces, in turn, a greater vortex spin and an attendant reduction in static pressure in the back cyclones relative to the two front cyclones. This will manifest itself as a difference in liquid level within the bottoms of the cyclones. We can perform some basic fluid flow analysis on the configuration shown in Fig. 13.B.1 and thereby gain some insight into the flow behavior therein.

We begin by regarding the inlet ducting feeding the six cyclones as being divided into six equal-area rectangular openings each of height h and width s, as shown in Fig. 13.B.2 below. For estimation purposes, we will use an equation describing the velocity profile in a circular duct to describe the lateral velocity profile in the rectangular ducting feeding the cyclones. Thus, the velocity v at a distance y from a sidewall is (Hinze, 1975).

$$\frac{v}{v_{max}} = \left(\frac{y}{3s}\right)^{\frac{1}{n}} \tag{13.B.1}$$

where v is the axial velocity a distance y from the side wall, v_{max} is the maximal axial velocity (at the entrance duct centerline), s is the width of each of the six entrance ducts, and

$$n = \frac{1}{\sqrt{f}} \tag{13.B.2}$$

where f is the Moody friction factor for the inlet duct.

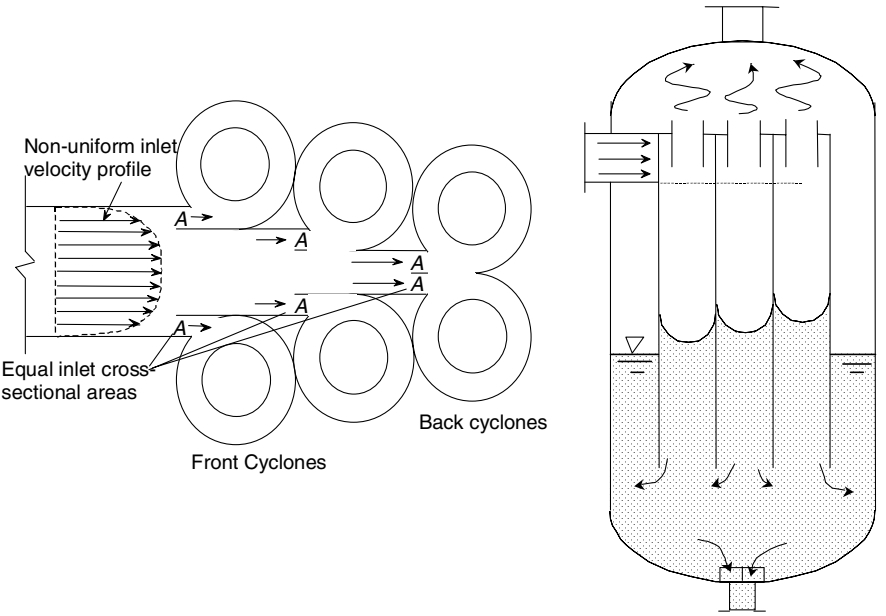

Fig. 13.B.1. Nonuniform entrance velocity profile (left frame) and associated static pressure difference (right frame) within a set of demisting cyclones

The flow to one 'front' cyclone is:

$$Q_F = \int_0^s vhdy = hv_{max} \int_0^s \left(\frac{y}{3s}\right)^{\frac{1}{n}} dy = \frac{hv_{max}}{3^{\frac{1}{n}} s^{\frac{1}{n}}} \left[\frac{y^{\frac{1}{n}+1}}{\frac{1}{n}+1}\right]_0^s = \frac{hsv_{max}}{3^{\frac{1}{n}}\left(\frac{1}{n}+1\right)}, \tag{13.B.3}$$

while the flow to one 'back' cyclone is:

$$Q_B = \int_{2s}^{3s} vhdy = 2hv_{max} \int_{2s}^{3s} \left(\frac{y}{3s}\right)^{\frac{1}{n}} dy = \frac{hv_{max}}{3^{\frac{1}{n}} s^{\frac{1}{n}}} \left[\frac{y^{\frac{1}{n}+1}}{\frac{1}{n}+1}\right]_s^{3s} = \frac{hsv_{max}}{3^{\frac{1}{n}}\left(\frac{1}{n}+1\right)} \left[3^{\frac{1}{n}+1} - 2^{\frac{1}{n}+1}\right]. \tag{13.B.4}$$

It is apparent from an inspection of Eqs. (13.B.3) and (13.B.4) that a back cyclone experiences a different volumetric flow rate than either of the two front cyclones. Since the inlet duct areas are the same for each cyclone, the ratio of these flow rates is also the same as the ratio of the average inlet velocities:

$$\frac{Q_B}{Q_F} = \frac{\langle v_B \rangle}{\langle v_F \rangle} = 3^{\frac{1}{n}+1} - 2^{\frac{1}{n}+1}. \tag{13.B.5}$$

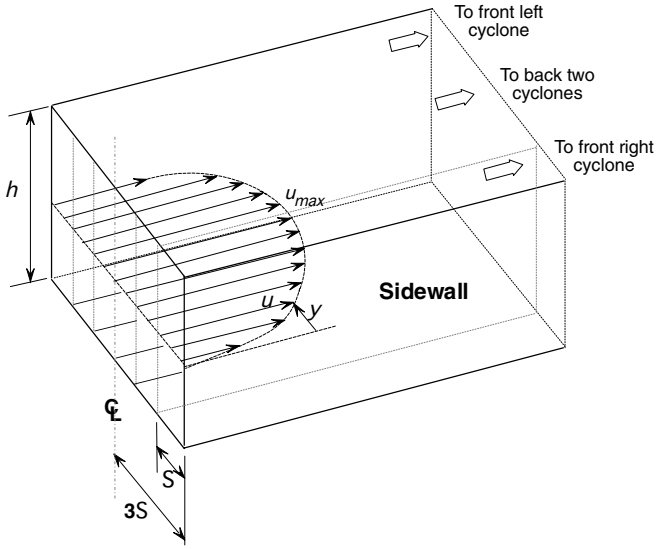

Fig. 13.B.2. Sketch illustrating the flow distribution upstream of a parallel array of demisting cyclones

And so we find that the imbalance is a function of the coefficient n or, according to Eq. (13.B.2), the friction factor, f. If the gas were not retarded by wall friction at all, then $f = 0$, n goes to infinity and the RHS of Eq. (13.B.5) becomes unity. This would correspond to an absolutedly flat velocity profile within the main inlet duct, and, hence, no inlet flow maldistribution.

The total pressure of the gas phase near the liquid surface, *i.e.*, the 'underflow' of either the front cyclones (subscript F) is:

$$p_{F,tot} = p_{F,static,duct} + p_{F,dynamic} - \Delta p_{F,in-uf}. \tag{13.B.6}$$

Likewise, the total pressure at the underflow of either back cyclone is:

$$p_{B,tot} = p_{B,static,duct} + p_{B,dynamic} - \Delta p_{B,in-uf} \tag{13.B.7}$$

where Δp_{in-uf} refers to the difference between cyclone inlet and underflow.

Subtracting Eq. (13.B.6) from (13.B.7) and canceling out the two static pressure terms gives the difference in pressure at the bottom (gas/liquid interface) between the front and back cyclone(s):

$$\Delta p = p_{B,dynamic} - p_{F,dynamic} - \Delta p_{B,in-uf} + \Delta p_{F,in-uf} \tag{13.B.8}$$

or,

$$\Delta p = \frac{1}{2}\rho\langle v_B\rangle^2 - \frac{1}{2}\rho\langle v_F\rangle^2 - \frac{1}{2}\rho K_{in-uf}\langle v_B\rangle^2 + \frac{1}{2}\rho K_{in-uf}\langle v_F\rangle^2 \tag{13.B.9}$$

with K_{in-uf} = inlet-to-underflow pressure loss coefficient. This coefficient must be computed from either a cyclone model or calculated on basis of measurements on an operating unit or on a laboratory model of the operating unit. The computation of K_{in-uf} requires one to measure or compute the inlet-to-underflow pressure difference, along with the gas density and average velocity in the upstream duct feeding one of the cyclones. Like the Euler number, it is a constant and has the same value for each of the cyclones, assumed herein to be physically identical in their construction.

Equation (13.B.9) can be simplified to give:

$$\Delta p = \frac{1}{2}\rho\,(1 + K_{in-uf})\ \left(\langle v_F\rangle^2 - \langle v_B\rangle^2\right). \tag{13.B.10}$$

Equation 13.B.10 will give a positive number if the pressure at the bottom of the back cyclone(s) is greater than that at the bottom of the front cyclone(s), and vice versa. The equation shows clearly that the difference in pressure between the bottoms of the front and back cyclones is dependent upon the difference in the square of the average velocity reporting to these cyclones. The two average inlet duct velocities in Eq. 13.B.10 are obtained by dividing the inlet volumetric flow rates from Eqs. (13.B.3) and (13.B.4) by the cross-sectional area of their inlet ducts, A. Doing so and substituting the results into Eq. 13.B.10 we obtain, after simplification:

$$\Delta p = \frac{\rho\,(\,1 + K_{in-uf})}{2}\left[\left(3^{\frac{1}{n}+1} - 2^{\frac{1}{n}+1}\right) - 1\right]^2 \left[\frac{v_{max}}{3^{\frac{1}{n}}\left(\frac{1}{n}+1\right)}\right]^2. \tag{13.B.11}$$

As before, the pressure difference shown here vanishes if there is no friction such that $n \to \infty$.

Obviously, the same sort of analysis and observations apply to any number of cyclone pairs whose underflows discharge into a common liquid seal pool. One just needs to work through the detailed computations on a case-by-case basis along the lines presented above.

In addition to vapor maldistribution, liquid maldistribution in the inlet piping will also give rise to a pressure imbalance within the bodies of front and back cyclones. This occurs because of the reduction in spin in the cyclone(s) that receive the greatest share of the liquid. This may not be a concern at the low liquid loadings typically associated with demisting type cyclones. At heavier loadings, however, one may need to modify the inlet piping to minimize liquid segregation ahead of the individual cyclones.

A worked example for estimation of the static pressure difference between demisting cyclones arising from inlet maldistribution is presented next.

13.B.1 Calculation of Flow Distribution

Given: An industrial demisting cyclone system consists of three pairs of identical cyclones which share a common hopper, as shown in Fig. 13.B.1. It is estimated that the wall friction factor in the ducting leading up to the cyclone is 0.019 or about 30% greater than that for gas-only.

Compute: The flow imbalance ratio according to Eq. (13.B.5).

Solution

Substituting our Moody friction factor into Eq. (13.B.2), we find that $n = 7.5$. This leads to the flow ratio: $Q_B/Q_F = \langle v_B \rangle / \langle v_F \rangle = 1.28$. Thus, due to the nonuniform velocity gradient in the inlet ducting, the back cyclones will experience about 30% more vapor flow than the two front cyclones. It is interesting to note that the computed value of the coefficient n, 7.5, is not too different from the 'Law of the Wall' coefficient of 7 often used to describe the velocity profile in fully developed turbulent flow within pipes.

13.B.2 Calculation of the Liquid Level Difference between the Front and Back Cyclones

Data for the cyclone system shown in Figs. 13.B.1 and 13.B.2 is as follows:

$\rho = 11.9$ kg/m^3
$K_{in-uf} = 2.6$ (based on a cyclone simulation study)
$f = 0.018$ (*i.e.*, $\cong$1.3 times f_{air})
$n = 7.5$
$v_{max} = \langle v \rangle / 0.80 = 18.2/0.80 = 22.8$ m/s (approximately)

Substituting these values into Eq. 13.B.11, we obtain a pressure difference between the back and front cyclones of about -0.224 kPa (about -23 mm or -1 inch of water column). Since this pressure differential (back - front) is negative, the liquid level in the two back cyclones will be 23 mm of water column higher than that for the two front cyclones. The level in the two middle cyclones can be expected to lie between that of the front and back cyclones.

Despite the rather large flow imbalance we found leading up to the entrance of the cyclones, this did not result in a significant difference in 'bottom' pressure among the cyclone pairs. However, as Eq. 13.B.11 shows, an increase in the gas density (as in high pressure separators) and/or the flow rate through the main inlet duct would increase the pressure and elevation differences reported above. Furthermore, if the liquid phase reporting to the bottom of the cyclones were to be a low-density foam or froth, the difference in their elevations would increase inversely with the decrease in the 'liquid's' effective density. If this foam column grew too high, it would become entrained overhead by the vortex and exit with the exiting gas phase.

Before closing this discussion we wish to call attention to the fact that the liquid seal at the bottom of each cyclone causes their performance to be rather unaffected by flow imbalances of the type we just observed. This would not be the case had the cyclone underflows not been isolated from one another. In this case, any pressure imbalance that would exist between the cyclone underflows will cause gas to flow down some of the underflow openings and up other underflow openings. This, in turn can lead to a serious degradation of separation performance and is the reason why most multiclone systems do not perform as well as one of its individual cyclones tested in isolation.

When faced with a cyclone performance problem it is almost always advisable to focus attention on the underflow configuration. The majority of performance problems are due, for one reason or the other, to the inability of particulates to properly discharge out the underflow openings.

13.C Method for Estimating Wall Film Thickness and Velocity

In some special applications it is of value to be able to estimate certain physical characteristics of the film of liquid that is flowing down the walls of a gas/liquid cyclone. This includes the fraction of the cross-sectional area occupied by the gas and by the liquid wall film, the film velocity, residence time, and film thickness. Such information is of interest, for example, in performing heat transfer computations wherein the wall film is heated by an external steam jacket, or the film is cooled by an external chilled water enclosure. Knowledge of the film characteristics is also of value if one is interested in ensuring that a sufficient film velocity or thickness is maintained to keep solids from depositing upon the walls. Herein, we shall present a technique that is intended to provide an estimate of the wall film's flow characteristics.

We saw in Sect. 13.7.1 that the tangential liquid film velocity and the liquid film thickness were required to calculate the reentrainment number. In that section these parameters were estimated by a method similar to that of Ishii and Grolmes (1975) by considering a force balance on the film resolved in the tangential direction. That model was geared to situations where reentrainment from a liquid may be important: high gas and liquid film velocities. Also the liquid film in that example was being transported upward against gravity, although the effect of gravity was not accounted for in the model. In this appendix we will derive an expression for the vertical velocity of a liquid film moving downward and the thickness of this film using a similar principle, but considering a force balance on the film resolved in the vertical direction. We will use different empirical expressions for the film-wall and gas-film friction factors, $f_{l,w}$ and $f_{g,i}$ to those used in Sect. 13.7.1, Eq. (13.7.8), and we will take into account the effect of gravity.

The model we develop in this appendix is thus based on a two-phase, cocurrent flow force balance that relates the cross-sectional liquid void fraction

(and, hence, the gas fraction) to the gas and liquid mass flow rates, physical properties, cyclone diameter, wall and interfacial friction factors, and the acceleration of gravity. We assume that all of the liquid entering the cyclone is spun to the walls immediately upon entry and flows down as a *uniformly* thick film[2], see Fig. 13.C.1.

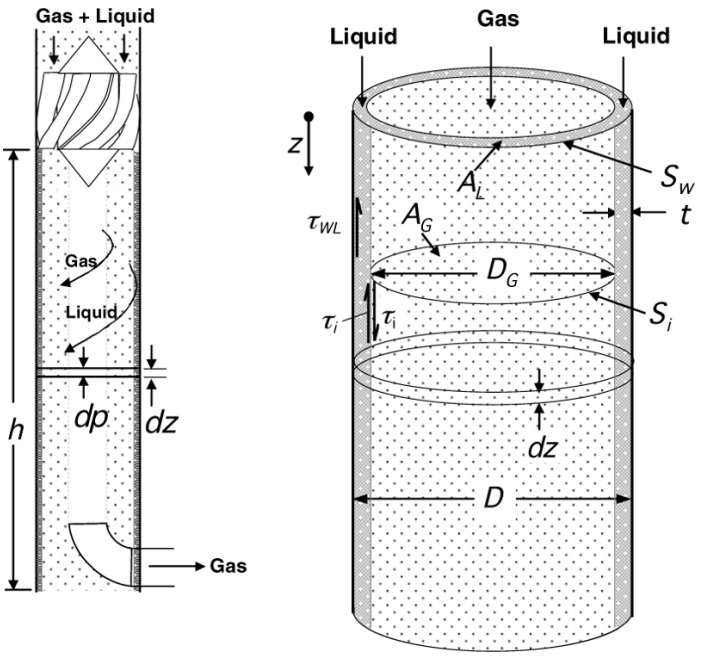

Fig. 13.C.1. Simplified view of cyclone with liquid film of thickness t along wall with gas comprising the core flow. Left image: cyclone overview. Right image: detail of a vertical segment of the cyclone

In *most* gas-liquid cyclone installations, the majority of all incoming liquid is deposited upon the walls immediately upon entry into the cyclone as a result of the "mass loading" effect alone. This is due to the relatively large size of the incoming liquid drops and also to the "mass loading effect" discussed in Sect. 13.6 above.

In this model, the primary purpose of the centrifugal force field generated by the rotational motion imparted to the incoming feed stream is to convey and keep the liquid on the walls of the cyclone. Herein we shall assume that the gas and liquid phases spiral down the walls of the cyclone in a helical

[2] A uniformly thick wall film is an idealized condition that is difficult to achieve in practice. A vane-type inlet with multiple openings (distribution points) generally provides a much more uniform distribution of the liquid than that of a slot or pipe type inlet.

fashion at a common, constant angle relative to the horizontal. We may view the flow as that over a flat plate created by unfolding the cylindrical walls of the cyclone. In this case, the gas and liquid flow paths are simply straight lines making a constant angle to the horizontal.

The force balance model equation that we shall derive below must be solved in an iterative manner for the vapor void fraction. Knowing this void fraction and the cyclone diameter, the wall film thickness can be computed. It is then possible to compute the average gas and wall film velocity, as well as the "slip velocity", the ratio of the average gas velocity to the average liquid film velocity.

13.C.1 Two-Phase, Co-current, Annular Force Balance, Resolved in the Axial Direction

We begin by performing a force balance in the axial z direction over a cross section of the cyclone of height dz. See Fig. 13.C.1. We shall assume that, for all practical purposes, all of the liquid is spiraling down the inner walls of the cyclone as a wall film with the gas phase comprising the core flow. A force balance on the gas phase gives (note that dp is itself negative),

$$-A_g dp - \tau_{g,i} \sin\alpha S_i dz + \rho_g A_g g dz = 0. \tag{13.C.1}$$

And that on the liquid phase,

$$-A_l dp - \tau_{l,w} \sin\alpha S_w dz + \tau_{g,i} \sin\alpha S_i dz + \rho_l g A_l dz = 0 \tag{13.C.2}$$

where A_g, A_l are the horizontal cross-sectional areas of gas and liquid wall film, respectively, dp is the axial pressure difference[3] across dz, $\tau_{g,i}$ and $\tau_{l,w}$ are the gas/liquid and wall/liquid shear stresses, respectively, α is the angle of the gas and liquid film flows (assumed here to be equal) relative to the horizontal, ρ_g, and ρ_l are the gas and liquid densities, S_i, S_w are the perimeters of gas core flow and the outer liquid film (the latter being the same as the inner wall perimeter), and g is the acceleration due to gravity.

Eliminating dp between Eqs. (13.C.1) and (13.C.2) and simplifying gives:

$$\frac{\tau_{l,w} \sin\alpha S_w}{A_l} - \tau_{g,i} \sin\alpha S_i \left(\frac{1}{A_g} + \frac{1}{A_l}\right) - (\rho_l - \rho_g) g = 0. \tag{13.C.3}$$

Now, if we name the fraction of the total cross-sectional area, $A = \pi D^2/4$, taken up by gas the "void fraction", ε, then $A_g = \varepsilon A$, $A_l = (1-\varepsilon)A$. Furthermore, we take the wetted wall perimeter, S_w, and the interface perimeter, S_i as $S_w = \pi D$ and $S_i = \pi D_g = \pi \varepsilon^{1/2} D$, respectively. Substituting this into Eq. (13.C.3) and simplifying gives:

$$\frac{4\tau_{l,w} \sin\alpha}{(1-\varepsilon) D} - \frac{4\tau_{g,i} \sin\alpha}{D\varepsilon^{1/2}(1-\varepsilon)} - (\rho_l - \rho_g) g = 0. \tag{13.C.4}$$

[3] We assume, as is normal, that the pressure in the gas permeates the liquid film

13.C.2 Friction Factors and Shear Stresses

In this section we give expressions for the wall and interfacial friction factors and corresponding shear stresses, starting with the wall friction factor and shear stress.

Wall Friction Factor and Shear Stress

By definition,

$$\tau_{l,w} \equiv \frac{1}{2}\rho_l \langle v_l \rangle^2 f_{l,w} \tag{13.C.5}$$

where $f_{l,w}$ can be computed by any number of correlations, among others those given in Eq (13.7.8). Herein we report two such correlations for $f_{w,l}$—that of Liang-Biao and Aziz (1996)—and that obtained using a conventional Moody type friction factor correlation (Swamee and Jain, 1976), with the Reynolds number defined in terms of an equivalent hydraulic diameter.

The correlation of Liang-Biao and Kaziz is:

$$f_{w,l} = \frac{1.629}{Re_l^{0.516}} \left(\frac{v_{s,g}}{v_{s,l}} \right)^{0.0926} . \tag{13.C.6}$$

We can rewrite the parameters in this equation as follows:

$$\begin{aligned}
v_{s,g} &= \text{superficial gas velocity } = \frac{\dot{m}_g}{\rho_g A} \\
v_{s,l} &= \text{superficial liquid velocity } = \frac{\dot{m}_l}{\rho_l A} \\
Re_l &= \text{liquid film Reynolds number} = \frac{\rho_l \langle v_l \rangle d_{Hl}}{\mu_l} \\
d_{Hl} &= \text{film hydraulic diameter} = \frac{4A_l}{S_w} = \frac{4\,(1-\varepsilon)\,A}{\pi D} = (1-\varepsilon)\,D
\end{aligned} \tag{13.C.7}$$

Furthermore the mean liquid velocity, $\langle v_l \rangle$ can be written:

$$\langle v_l \rangle = \frac{\dot{m}_l}{\rho_l A_l} = \frac{\dot{m}_l}{\rho_l\,(1-\varepsilon)\,A} = \frac{4\dot{m}_l}{\rho_l\,(1-\varepsilon)\,\pi D^2} \tag{13.C.8}$$

with $\dot{m}_l$ and $\dot{m}_g$ the liquid and gas mass flowrates.

Substituting these expressions into eq. (13.C.6) gives:

$$f_{l,w} = \frac{1.629}{\left(\frac{4\dot{m}_l}{\pi D \mu_l}\right)^{0.516}} \left(\frac{\rho_l \dot{m}_g}{\rho_g \dot{m}_l} \right)^{0.0926} \tag{13.C.9}$$

An alternative method for estimating the wall friction factor is to use a standard pipe friction factor equation, such as the explicit formula of Swamee and Jain, using the equivalent diameter of the film in Re_l. Thus,

$$f_{l,w} = \frac{0.25}{\left[Log_{10}\left(\frac{e}{3.7D} + \frac{5.74}{Re_l^{0.9}}\right)\right]^2} \tag{13.C.10}$$

where e is the conventional absolute wall roughness. Re_l, and the equivalent diameter comprising part of Re_l, are given in Eq. (13.C.7) above.

Using the expression for $\langle v_l \rangle$ in Eq. (13.C.7) in the definition for the wall shear stress, $\tau_{l,w}$, Eq. (13.C.5), gives:

$$\tau_{l,w} = \frac{8\dot{m}_l^2}{\pi^2 D^4 \rho_l \left(1-\varepsilon\right)^2} f_{l,w} \tag{13.C.11}$$

where $f_{l,w}$ is computed by either Eq. (13.C.9) or (13.C.10).

Interfacial Friction Factor and Shear Stress

Similar to the wall shear stress, the interfacial shear stress is defined as:

$$\tau_{g,i} \equiv \frac{1}{2}\rho_g \langle v_g \rangle^2 f_{g,i} \tag{13.C.12}$$

For turbulent gas flow $f_{g,i}$ may be computed from some empirical function of the gas Reynolds number, as outlined below.

Zhao and Liao (2002) proposed the following formula for computing the gas/liquid interfacial friction factor for annular flow:

$$f_{g,i} = 0.046 Re_g^{-0.2} \tag{13.C.13}$$

where Re_g, the gas Reynolds number, is defined as:

$$Re_g \equiv \frac{\rho_g \langle v_g \rangle D_g}{\mu_g}. \tag{13.C.14}$$

$\langle v_g \rangle$, the mean gas velocity, can be written:

$$\langle v_g \rangle = \frac{\dot{m}_g}{\rho_g A_g} = \frac{\dot{m}_g}{\rho_g \varepsilon A} = \frac{4\dot{m}_g}{\rho_g \varepsilon \pi D^2} \tag{13.C.15}$$

Substituting Eq. (13.C.15) into Eq. (13.C.14), and noting that the diameter of the region available for gas flow, $D_g = \varepsilon^{1/2} D$:

$$Re_l = \frac{4\dot{m}_g}{\pi \mu_g \varepsilon^{1/2} D} \tag{13.C.16}$$

Thus, Eq. (13.C.13) becomes,

$$f_{g,i} = 0.046 \left(\frac{4\dot{m}_g}{\pi \mu_g \varepsilon^{1/2} D}\right)^{-0.2} \tag{13.C.17}$$

Filling the expression in Eq. (13.C.15) for the mean gas velocity, $\langle v_g \rangle$, into Eq. (13.C.12) gives:

$$\tau_{g,i} = \frac{8\dot{m}_g^2}{\rho_g \varepsilon^2 \pi^2 D^4} f_{g,i} \tag{13.C.18}$$

where $f_{g,i}$ is computed from Eq. (13.C.17). We note that Eq. (13.C.18) is very similar to Eq. (13.C.11).

13.C.3 Final Form of Void Fraction Equation

Substituting the shear stresses, $\tau_{g,i}$ and $\tau_{l,w}$, from Eqs.(13.C.11) and (13.C.18) into the force balance equation, Eq. (13.C.4), and simplifying, we obtain an implicit expression relating void fraction to known quantities such as cyclone diameter, gas and liquid mass flow rates, gas and liquid densities and viscosities, and the acceleration of gravity:

$$\frac{32 \sin\alpha}{\pi^2 D^5 (1-\varepsilon)} \left[\frac{\dot{m}_l^2}{\rho_l (1-\varepsilon)^2} f_{l,w} - \frac{\dot{m}_g^2}{\rho_g \varepsilon^{5/2}} f_{g,i} \right] - (\rho_l - \rho_g) g = 0 \tag{13.C.19}$$

where $f_{l,w}$ and $f_{g,i}$ are given by Eqs. (13.C.9) or (13.C.10), and (13.C.17).

Equation (29) must be solved iteratively for the void fraction, ε, as a function of the independent quantities:

$$\dot{m}_l,\ \dot{m}_g,\ \rho_l,\ \rho_g,\ \mu_l,\ \mu_g,\ D,\ f_{l,w},\ f_{g,i} \text{ and } g\ .$$

Once ε is known for a given set of local conditions, it is then possible to compute the liquid phase fraction $(1-\varepsilon)$, the film thickness, t, the film and gas phase velocities, v_l and v_g, and the slip velocity, v_{slip}.

Knowing ε and the cyclone diameter, D, the film thickness, t, for any value of ε can now be computed,

$$t = \frac{D(1-\sqrt{\varepsilon})}{2}, \tag{13.C.20}$$

which follows from the fact that

$$1 - \varepsilon = \frac{A_l}{A} = \frac{\frac{\pi}{4}D^2 - \frac{\pi}{4}(D-2t)^2}{\frac{\pi}{4}D^2}$$

An estimate of the residence time of the liquid film over cyclone height H can be obtained by dividing its helical path length, $H/\sin\alpha$, by the film velocity v_l,

$$\theta_{l\_res} \cong \frac{H}{v_l \sin\alpha}.$$

Due to friction and the effects of gravity, the angle at which the liquid film flow relative to the horizontal, α_l, will increase somewhat over the length of the cyclone. Lacking direct measurements an average value of 45° to 55°

is suggested, basis observation. If the feed enters the cyclone through a vane assembly, the initial or starting angle will be fixed by the angle of the trailing section of the vanes (typically $\sim 20°$ to $30°$). If the feed enters through a tangential inlet (slot or round pipe), the starting angle will be approximately $30°$. Near the bottom of the cyclone, the angle typically increases to $45°$ to $60°$ as a result of wall friction and the effects of gravity.

The vertical "slip velocity", defined as the ratio

$$v_{slip} \equiv \frac{\langle v_g \rangle}{\langle v_l \rangle} \tag{13.C.21}$$

becomes, with the help of Eqs.(13.C.8) and (13.C.15),

$$v_{slip} \equiv \frac{\langle v_g \rangle}{\langle v_l \rangle} = \frac{\rho_l}{\rho_g} \times \frac{\dot{m}_g}{\dot{m}_l} \times \frac{(1-\varepsilon)}{\varepsilon A} \tag{13.C.22}$$

Although the two mean velocities differ, there is no discontinuity (no "slip") at their interface.

13.D Example calculation

For the purpose of illustrating the use of the above formulas, we'll go through the calculations for computing the wall film thickness, velocity, residence time and slip velocity for a commercial scale cyclone designed to separate an aqueous phase from an air stream.

$\dot{m}_l$	= 30,000 lb/hr	= 3.78 kg/s
$\dot{m}_g$	= 150,000 lb/hr	= 18.9 kg/s
α_l	$\cong 40°$	
D	= 30.0 in	= 0.762 m
H	= 48.0 in	= 1.219 m
ρ_l	= 62.4 lb/ft^3	= 1000 kg/m^3
ρ_g	= 0.150 lb/ft^3	= 2.40 kg/m^3
μ_l	= 1.00 cp	= 0.001 Pa·s
μ_g	= 0.040 cp	= 4.0×10^{-5} Pa·s

Wall friction factor according to Liang-Biao and Kaziz:

$$f_{l,w} = \frac{1.629}{\left(\frac{4\dot{m}_l}{\pi d \mu_l}\right)^{0.516}} \left(\frac{\rho_l \dot{m}_g}{\rho_g \dot{m}_l}\right)^{0.0926}$$

$$= \frac{1.629}{\left(\frac{4 \cdot 3.78}{\pi 0.762 \cdot .001}\right)^{0.516}} \left(\frac{1000 \cdot 18.9}{2.40 \cdot 3.78}\right)^{0.0926} = 0.0362$$

Wall friction factor according to Swamee and Jain:

$$d_{Hl} = (1-\varepsilon)D = (1-\varepsilon)0.762$$

$$\langle v_l \rangle = \frac{4\dot{m}_l}{\rho_l(1-\varepsilon)\pi D^2} = \frac{4 \times 3.78}{\pi 1000(1-\varepsilon)0.762^2} = \frac{0.00829}{1-\varepsilon}$$

$$Re_l = \frac{\rho_l \langle v_l \rangle d_{Hl}}{\mu_l} = \frac{1000 \times 0.00829 \times 0.762}{0.001} = 6317$$

e = wall roughness = 0.0018 in. = 0.000046 m

$$f_{l,w} = \frac{0.25}{\left[\log_{10}\left(\frac{e}{3.7D} + \frac{5.74}{Re_l^{0.9}}\right)\right]^2} = \frac{0.25}{\left[\log_{10}\left(\frac{0.000046}{3.7 \times 0.762} + \frac{5.74}{6317^{0.9}}\right)\right]^2} = 0.0354$$

Interfacial friction factor according to Zhao and Liao:

$$f_{g,i} = 0.046\left(\frac{4\dot{m}_g}{\pi\mu_g\varepsilon^{1/2}D}\right)^{-0.2}$$

$$= 0.046\left(\frac{4 \times 18.9}{\pi\, 4.0 \times 10^{-5}\varepsilon^{1/2}0.762}\right)^{-0.2} = 0.00304\varepsilon^{0.1}$$

Substituting into our force balance equation (using only the Swamee and Jain value for $f_{l,w}$):

$$\frac{32\sin\alpha}{\pi^2 D^5(1-\varepsilon)}\left(\frac{\dot{m}_l^2}{\rho_l(1-\varepsilon)^2}f_{l,w} - \frac{\dot{m}_g^2}{\rho_g\varepsilon^{5/2}}f_{g,i}\right) - (\rho_l - \rho_g)g = 0$$

$$\frac{32\sin 40}{\pi^2 0.762^5(1-\varepsilon)}\left(\frac{3.78^2}{1000(1-\varepsilon)^2}0.0354 - \frac{18.9^2}{2.40\varepsilon^{5/2}}0.00304\varepsilon^{0.1}\right)$$

$$- (1000 - 2.40)9.81 = 0$$

or

$$\frac{0.004104}{(1-\varepsilon)^3} - \frac{3.670}{(1-\varepsilon)\varepsilon^{2.4}} - 9786 = 0$$

By trial and error,

$$\varepsilon = 0.99264$$

In this particular example, wall friction and gravity are controlling; interfacial friction has a relatively minor effect on the film's thickness, velocity and residence time (computed below).

The wall film thickness is therefore,

$$t = \frac{d\,(1-\sqrt{\varepsilon})}{2} = \frac{0.762\left(1-\sqrt{0.99264}\right)}{2} = 0.00140 \text{ m } = 1.40 \text{ mm}$$

The vertical wall film velocity is,

$$\langle v_l \rangle = \frac{4\dot{m}_l}{\rho_l (1-\varepsilon)\pi D^2} = \frac{4 \times 3.78}{1000\,(1-0.99264)\,\pi 0.762^2} = 1.13 \text{ m/s } (3.71 \text{ ft/s})$$

The slip velocity is,

$$v_{slip} \equiv \frac{\langle v_g \rangle}{\langle v_l \rangle} = \frac{\rho_l}{\rho_g} \times \frac{\dot{m}_g}{\dot{m}_l} \times \frac{(1-\varepsilon)}{\varepsilon A} = \frac{1000}{2.40} \times \frac{18.9}{3.78} \times \frac{(1-0.99264)}{0.99264 \times \frac{\pi}{4} 0.762^2} = 33.9$$

The liquid film residence time is,

$$\theta_{l\_res} \cong \frac{H/\sin 40}{v_L} = \frac{1.219}{1.13} = 1.68 \text{ s}$$

As a final note, we must bear in mind that the wall film within a gas-liquid cyclone does not normally spread out as a uniformly thick film. Instead, the liquid tends to segregate somewhat even though all areas of the walls may still be wetted. In order to achieve even a reasonable approach to uniform wall wetting, it is necessary for the feed stream to pass through a vane type inlet assembly having a multitude of vane openings (8 to 12, for example). It is also necessary that the liquid be distributed uniformly upstream of the vane. In general, the liquid film's average velocity will be greater than, and its actual residence time less than, that computed by the above method due to segregation.